Available online at www.sciencedirect.com
ScienceDirect
Cement and Concrete Research 38 (2008) 565–574
Cement and Concrete Research

Drying and autogenous shrinkage of pastes and mortars with activated slag cement

Antonio A. Melo Neto [a], Maria Alba Cincotto [a,*], Wellington Repette [b]

[a] Department of Civil Construction Engineering, University of Sao Paulo (USP), Av. Prof. Almeida Prado 83, Zip Code 05508-900 Sao Paulo, Sao Paulo, Brazil
[b] Department of Civil Engineering, Federal University of Santa Catarina, Zip Code 88040-900 Florianópolis, Santa Catarina, Brazil

Received 9 February 2007; accepted 1 November 2007

Abstract

Activated slag cement (ASC) shows significantly higher shrinkage than ordinary Portland cement agglomerates. Cracking generated by shrinkage is one of the most critical drawbacks for broader applications of this promising alternative binder. This article investigates the relationship between ASC hydration, unrestrained drying and autogenous shrinkage of mortar specimens. The chemical and microstructure evolution due to hydration were determined on pastes by thermogravimetric analysis, conduction calorimetry and mercury porosimetry. Samples were prepared with ground blast furnace slag (BFS) activated with sodium silicate (silica modulus of 1.7) with 2.5, 3.5 and 4.5% of Na_2O, by slag mass. The amount of activator is the primary influence on drying and autogenous shrinkage, and early hydration makes a considerable contribution to the total result, which increases with the amount of silica. Drying shrinkage occurred in two stages, the first caused by extensive water loss when the samples were exposed to the environment, and the second was associated with the hydration process and less water loss. Due to the refinement of ASC porous system, autogenous shrinkage is responsible for a significant amount of the total shrinkage.

Keywords: Shrinkage; Autogenous; Alkali activated cement; Pore size distribution; Thermal analysis

1. Introduction

The development of new materials and technologies for absorbing residues is an important mission for the cement industry, and of the various residues investigated; blast furnace slag (BFS) plays a very important role. Even though the cement industry consumes large quantities of slag, there is still a great volume available for use as an alternative binder. The thermal transformation of CaO, which is the main constituent of clinker in the production of cement, consumes an enormous amount of fuel and energy. As 1 ton of clinker generates approximately the same amount of CO_2 [1], the large scale production of Portland cement is a significant source of atmospheric pollution [2]. Therefore, the use of the slag as concrete and mortar binder can be less expensive and an ecologically friendly alternative.

Activated slag cement (ASC) is a blend of blast furnace slag and activators, which are chemical species capable of enhancing slag reactivity during hydration. When compared with normal Portland cement, sodium silicate ASC presents higher strengths, lower porosity and heat evolution, but increased shrinkage [3,4]. The elaboration of ASC compositions that develop mechanical properties extremely fast [4,5] making them advantageous for reducing operational downtimes, such as during the repair of roads or industrial structures. ASC hydrated products are highly resistant to chemical attacks, especially under acidic conditions [6,7], which makes them suitable as the binder for protecting overlay formulations. When comparing prices of raw materials in Brazil, ASC becomes an economically advantageous alternative for applications where ordinary normal Portland cement is used.

Activated slag cement shrinkage is larger than that of Portland cement and this could represent the most serious limitation for the dissemination of its use [8–10]. Different studies have identified the main parameters involved with ASC

* Corresponding author. Tel.: +55 11 3091 5792; fax: +55 11 3091 5544.
E-mail address: maria.cincotto@poli.usp.br (M.A. Cincotto).

0008-8846/$ - see front matter © 2007 Elsevier Ltd. All rights reserved.
doi:10.1016/j.cemconres.2007.11.002

Table 1
Blast furnace slag chemical composition

Component	Weight percent
SiO_2	33.78
Al_2O_3	13.11
CaO	42.47
MgO	7.46
Fe_2O_3	0.51
K_2O	0.32
Na_2O	0.16
SO_3	0.15
S^{2-}	1.14
Free lime	0.1
LOI	1.67
Insoluble residue	0.53

shrinkage, namely, the chemical activator specie and dosage [11–13]; BFS fineness [14]; and the curing conditions [15]. In general, shrinkage increases with higher dosages of activator and BFS fineness. This is also true for sodium silicate (waterglass) based activators when compared with sodium hydroxide and sodium carbonate based materials.

The shrinkage of sodium silicate ASC is not satisfactorily understood, particularly regarding (a) intensity, evolution with time, effect of activator type and dosage, (b) the correlation between shrinkage and hydration evolution, (c) the correlation between drying shrinkage and mass change, and (d) the development and contribution of autogenous shrinkage to the total shrinkage. The understanding of shrinkage development and its relationship to the evolution hydration is essential for the selection of adequate alternatives for reducing shrinkage, such as the use of shrinkage compensating (SCA) and shrinkage reducing admixtures (SRA). Since shrinkage normally occurs at very early ages, it may be responsible for the early age cracking reported for ASC based elements.

This article reports on the study of drying and autogenous shrinkage of sodium silicate ASC having 2.5, 3.5 and 4.5% of Na_2O, with an emphasis on the evolution of shrinkage and its relation to chemical and microstructure characteristics during the hydration process.

Table 2
Blast furnace slag physical characteristics

Physical characteristics
Density: 2.88 g/cm^3
Blaine finesses: 500 m^2/kg
Specific surface area (laser granulometry): 493 m^2/kg
Average particle diameters
D_{10}=2.22 μm D_{50}=11.87 μm D_{90}=32.37 μm $D_{[4,3]}$=14.99 μm $D_{[3,2]}$=4.59 μm

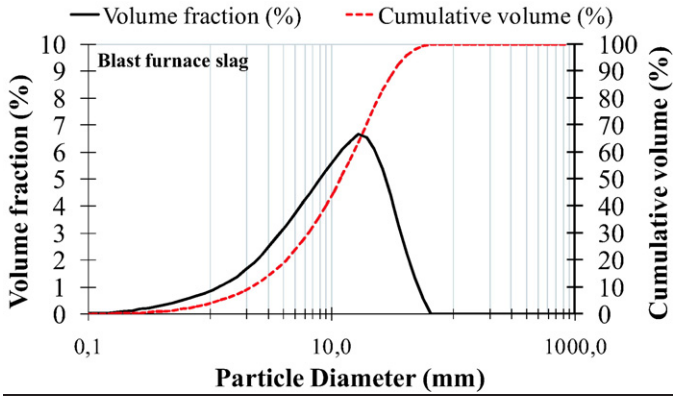

Table 3
Percentage by weight corresponding to sand granulometry fractions (mm)

>4.8 mm	4.8 mm–2.4 mm	2.4 mm–1.2 mm	1.2 mm–0.6 mm	0.6 mm–0.3 mm	0.3 mm–0.15 mm	<0.15 mm
0	0	25	25	25	25	0

2. Experimental

2.1. Materials and mix proportion of mortars and pastes

The granulated blast furnace slag was supplied by Companhia Siderúrgica de Tubarão, with a basicity coefficient Kb=(CaO+MgO)/(SiO_2+Al_2O_3)=1.06. The slag consisted of 99.5% glass and some crystalline components such as gehlenite and merwinite, with its chemical composition presented in Table 1 and physical characteristics in Table 2. The aggregate used was quartz sand (density=2.62 g/cm^3) composed of four equal proportions of the fractions sieved (Table 3).

Mortar samples were prepared with a mass proportion of cementitious binder:sand:water of 1:2:0.48, while the paste samples were prepared with mass proportion of 1:0.48. The cementitious binder corresponds to the total mass of slag and the solid fraction of the activator combined; the water contained in the activators (Table 4) was deducted from the total amount of water. The ground blast furnace slag was activated with sodium silicate having silica modulus (SiO_2/Na_2O) of 1.7, with 2.5, 3.5 and 4.5% of Na_2O, by slag mass. The activators and their composition are summarized in Table 5. Mortar and paste samples were labeled in accordance with the type of activator.

2.2. Testing methods

2.2.1. Shrinkage tests

Nine mortar prisms measuring 25×25×85 mm were cast for each binder. Drying and autogenous shrinkage tests were performed at ages, 6, 8, 10 and 12 h, 1, 2, 3, 4, 5, 6, 7, 9, 11, 14, 21 and 28 days. Length and mass variances were validated in accordance with ASTM C490. The method of testing involved measurement using a length comparator of the linear dimension variation of a specimen along the longitudinal axis. All prisms were wrapped with an inner layer of plastic and an outer layer of aluminum foil, sealed with aluminum tape. Recorded maximum moisture loss at 56 days was 0.2%. The prisms were demoulded at 6 h for the autogenous and drying shrinkage tests and immediately stored in a drying room at a constant temperature of 24 °C and 50% RH. The maximum increase in temperature due to heat released during hydration was 3 °C. The results of

Table 4
Sodium silicate chemical composition

Component	Weight percent
Na_2O	16.70
SiO_2	28.40
H_2O	54.90

Table 5
Composition of activators

Name	Type	Composition	Silica modulus
2NS	Sodium silicate	$2.5\%Na_2O+4.25\%SiO_2$	1.7
3NS		$3.5\%Na_2O+5.95\%SiO_2$	1.7
4NS		$4.5\%Na_2O+7.65\%SiO_2$	1.7

drying and autogenous tests were corrected for temperature effects using a thermal expansion coefficient equal to 15×10^{-6}/°C.

2.2.2. Hydration evolution tests

Changes in hydrated compounds and microstructure due to the evolution of hydration were determined in paste samples prepared with a water/binder ratio of 0.48. The arrest of hydration took place by freezing the samples in liquid nitrogen, followed with liofilization for water removal. For each mix, samples were prepared at hydration ages of 6, 8, 10, and 12 h and 1, 2, 3, 7, 14, and 28 days. Thermogravimetric curves were obtained using a NETSZCH TG 209-C thermobalance, with a heating ratio of 10 °C/min and under a nitrogen atmosphere with a gas flux of 30 ml/min. For this test, samples were first ground, and only the particles retained between the sieves with mesh 75 μm and 150 μm, were used. Pore size distribution was determined using a Micromeritics Autopore III 9410 porosimeter under pressures ranging from zero to 414 MPa. The assumed surface tension of the mercury was 0.485 N/m at 25 °C (ASTM D 4404-84). The density of the mercury was 13.5413 g/ml and the assumed contact angle was 130°. For the calorimetry tests, samples of paste were prepared by mixing 20 g of slag and water+activator in a plastic bag before being immediately transferred to a JAF Wexham conduction calorimeter at 20 °C. The compressive strength for the same samples were tested and already published [3,16] and the results at 28 days for 4NS, 3NS and 2NS were 96 MPa, 76 MPa and 27 MPa. Flexural strengths at 28 days for 4NS, 3NS and 2NS were 10 MPa, 9 MPa and 5 MPa, respectively.

3. Results and analyses

3.1. Conduction calorimetry

Fig. 1(a) shows the profile of heat evolution during the first 72 h. Slag solubility influences the reactions sequence, and the total cumulative heat diminishes as the quantity of Na_2O decreases. The induction period increases and the magnitude of the peak corresponding to the main products formation decreases as the amount of Na_2O decreases. This is evidence of the effect of the alkaline media on solubility of the slag and the hydration evolution (Fig. 1(b)). Due to the silica modulus being constant, the logical conclusion is that the degree of reaction increases with the amount of silica.

3.2. Thermogravimetry analyses

The results of TGA analysis curves indicate the presence of a mass peak loss between 30 °C and 220 °C, attributed to C–S–H (I) and aluminates; a smooth mass peak loss related to decomposition of hydrotalcyte between 275 °C and 425 °C, and the occurrence of a mass peak loss due to the decomposition of calcium carbonate, at temperatures around 700 °C. A typical TGA result is presented in Fig. 2, and corresponds to the results obtained for the mixtures at 28 days.

The estimated amount of C–S–H (I) was a function of hydration time and the amount of sodium silicate activators (Fig. 3, with details in Fig. 4). The amount of C–S–H increases as the amount of sodium silicate is increased. It is possible to conclude that C–S–H formation does not depend entirely on the alkalinity proportioned by the activator (which provides dissolution of slag), but also on the availability of silicate ions, supplied by the activator. Thus, if the silica modulus is

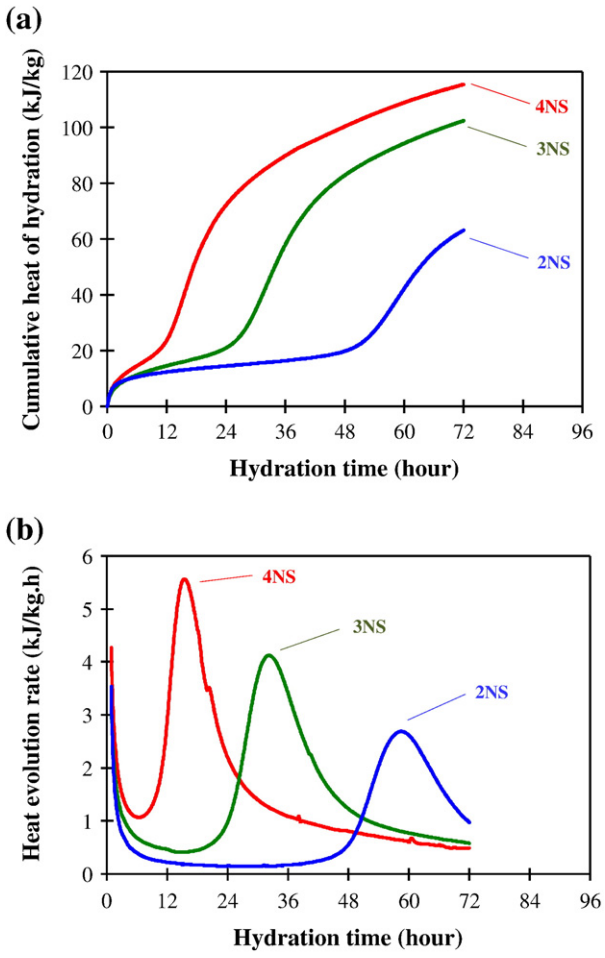

Fig. 1. Cumulative heat of hydration (a) and heat evolution rate (b) of ASC pastes.

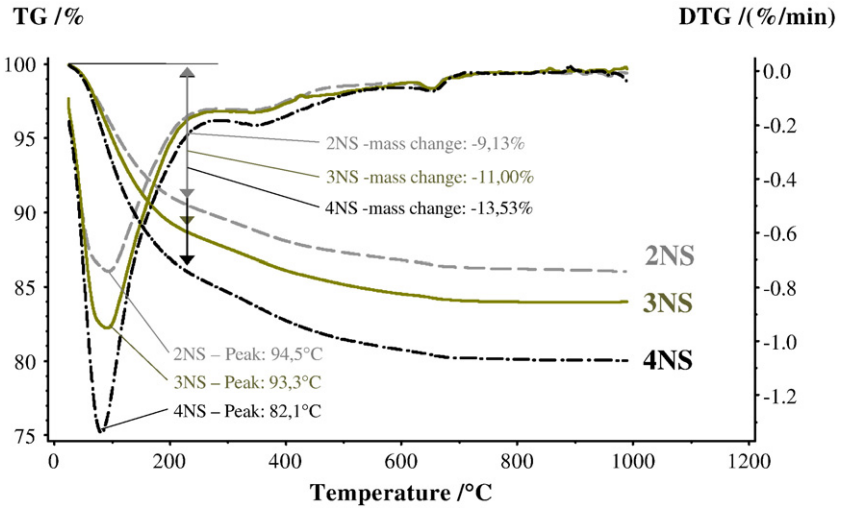

Fig. 2. TG and DTG curves of ASC pastes hydrated for 28 days.

kept constant, the degree of hydration increases as the amount of sodium silicate increases.

3.3. Porosity

In Fig. 5(a), the cumulative curves of pore size distribution show a different profile of ASC mixtures activated with different amounts of sodium silicate. The total volume of pores at 28 days follows the order: 2NS>3NS>4NS. The incremental pore size curves show the quantitative distribution frequency of the pore sizes in the range of mesopores and macropores (Fig. 5(b)). The 4NS and 3NS are practically unimodal and the 2NS is bimodal. This indicates that silica plays an important role in the densification of gel, maximum pore sizes being 25 nm for the 3 N mix and 15 nm for the 4 N mix. The volume of pores for ASC in the mesopores size range tends to be higher than that of ordinary Portland cement [17]. Mesopores account for 90–95% of the total pore volume for the silicate mixes. The threshold diameter represents the pore network of the sample which can be estimated to determine the diameter at which porosity starts to increase sharply as pore diameters decrease. The threshold diameter is in the region of mesopores, whose value diminishes as the amount of silica content increases. The results obtained are in agreement with other studies on ASC porosity [11,18,19]. Fig. 6 shows the evolution of the total porosity up to 28 days of age. An increase in the amount of sodium silicate reduces total porosity, which possibly, occurs due to the more intense hydration which results from the increase in sodium silicate, as confirmed by the results of thermogravimetric analysis. Fig. 7 shows the evolution of total porosity up to 48 h. It is observed that a decrease in the amount of sodium silicate retards the beginning of pore refinement.

3.4. Drying and autogenous shrinkage

The plotted curves in Figs. 8 and 9 correspond to the average drying and autogenous shrinkage results of nine replicate specimens for each mix. The cumulative drying and autogenous shrinkage for all activated slag mixes are high and increase with the content of sodium silicate. Most of the total drying and autogenous shrinkage take place during the early ages.

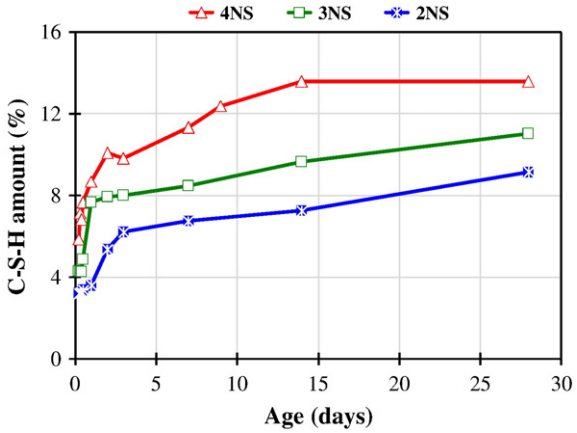

Fig. 3. Influence of activator content on C–S–H amount.

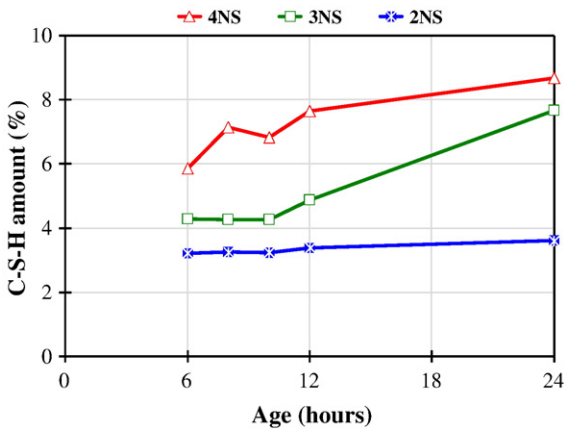

Fig. 4. Influence of activator content on C–S–H amount in the first 24 h.

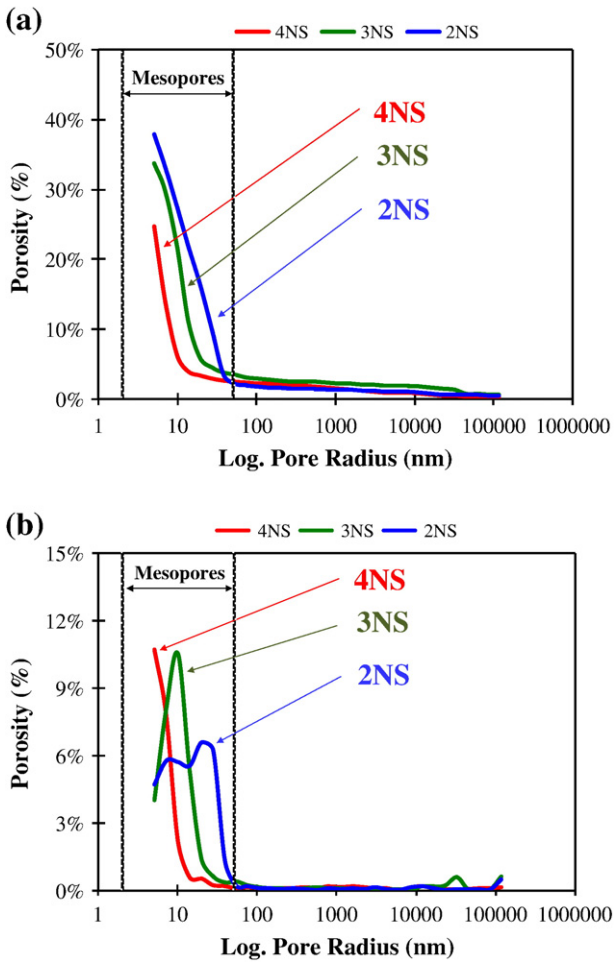

Fig. 5. Cumulative (a) and incremental (b) pore size distribution of ASC pastes hydrated for 28 days.

Autogenous shrinkage increases with the quantity of SiO_2, but the difference between mixes 3NS and 2NS is only statistically significant (p-value 0.05) up to 21 days [3]. The statistical data for the mixtures are presented in Table 6. The amount of sodium silicate activator greatly influences mechanical properties, porosity and the degree of hydration, which are determining factors for the evolution of autogenous shrinkage [3,17]. An increase of sodium silicate caused the decrease of the total porosity and the increase of mesopores volume, which is directly related with the shrinkage due to self-desiccation. Moreover, the degree of hydration increases as the amount of activator increases and the autogenous shrinkage related to chemical shrinkage also increases.

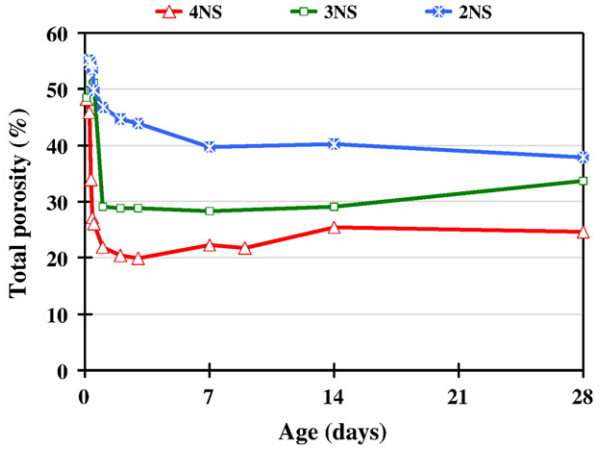

Fig. 6. Influence of activator content on total porosity of ASC pastes.

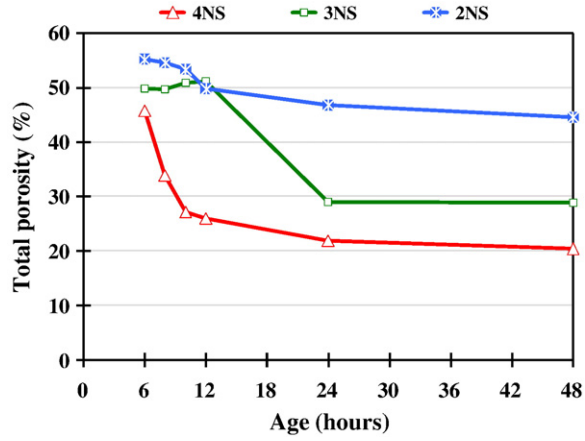

Fig. 7. Influence of activator content on total porosity of ASC pastes in the first 24 h.

Chemical shrinkage is a reduction in volume resulting from the chemical reaction between the reagent and water. Chen and Brouwers [20] studied the application and adaptation of activated slag cement experimental results in some reaction models for quantifying the hydrated products, chemical shrinkage and porosity. They conclude that C–S–H is the major hydrated product (around 92%), which, as already observed in thermogravimetric results presented in this article. The results from the chemical shrinkage of ASC demonstrate it is around 12–14 ml/100 g, which is much higher than that of Portland cement (approx. 6–10 ml/100 g) [21]. Thermogravimetric analysis indicates that an increase in the amount of sodium silicate intensifies hydration which leads to an increase in the total amount of chemical shrinkage.

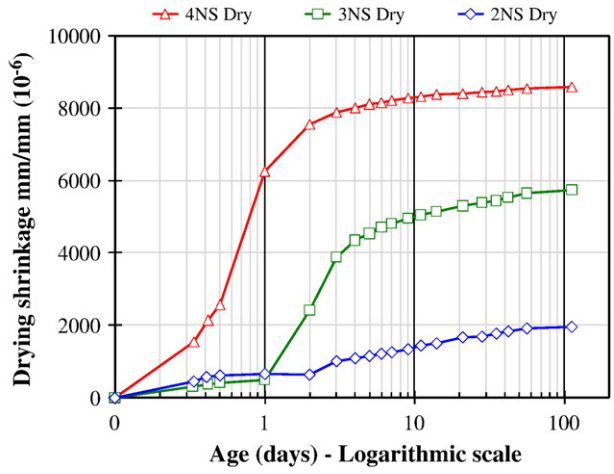

Fig. 8. Drying shrinkage of ASC mortars.

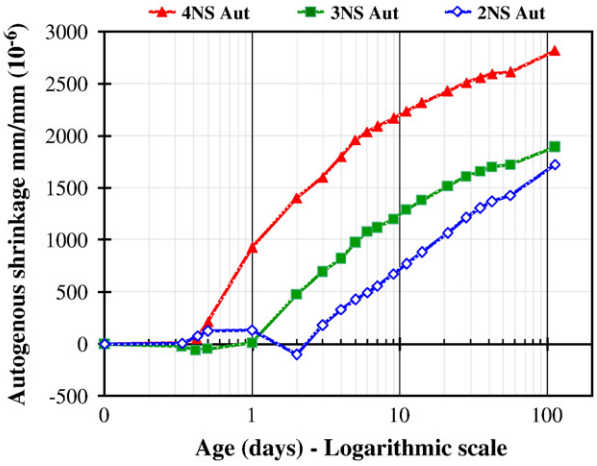

Fig. 9. Autogenous shrinkage of ASC mortars.

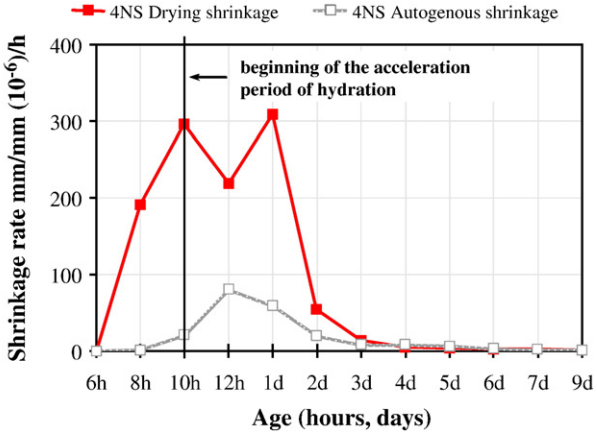

Fig. 10. Drying and autogenous shrinkage rates of 4NS mortars.

Hydration leads to an increase in the number of empty pores within the material. Porosity, pore size distribution and pore interconnectivity have a considerable influence on the mechanical properties of the paste. Chen and Brouwers [20] obtained results in agreement with the ones presented in this article. According to the results obtained in predicted model, the total porosity of ASC is near or lower than that of Portland cement; however, the pore size distribution of ASC is characterized by a high volume of gel pores. By using the predict models, the authors obtained a total porosity of around 35% for ASC, of which, gel pores accounted for 72%. Autogenous shrinkage may be defined as the macroscopic result of the effects of chemical shrinkage and self-desiccation. Therefore, the intense autogenous shrinkage of ASC can be attributed to the very high amount of chemical shrinkage and high capillary pressure resulting from self-desiccation. In this case, self-desiccation is most likely greater than that found in Portland cement and increases due to the amount of sodium silicate. The results from porosimetry testing support this affirmation. As previously stated, increasing the amount of sodium silicate resulted in a decrease in total porosity, and simultaneously, an increase in pore size refinement.

An enhanced interpretation of shrinkage evolution appears in the initial ages through the shrinkage rate that corresponds to the relationship between shrinkage variation and the elapsed time corresponding to the reading interval. Figs. 10–12 present measured drying and autogenous shrinkage rates for the ASC mixtures. The results show that both drying and autogenous shrinkage evolve in two distinct stages, before and at the start of the acceleration period of hydration. All mixtures present a peak in the curves of the autogenous shrinkage rate after the formation of hydrated products, attributed to chemical shrinkage and self-desiccation. Contrastingly, before the acceleration

Table 6
Drying and autogenous shrinkage statistical data for the 2NS, 3NS and 4NS mortars

		7 days	21 days	28 days	56 days	112 days
Drying shrinkage						
2NS mixture	Mean (mm/mm × 10^{-6})	1249.9	1660.5	1680.0	1906.2	1960.9
	Standard deviation (mm/mm × 10^{-6})	134.6	158.5	160.2	162.0	169.8
	Coefficient of variation (%)	10.8	9.5	9.5	8.5	8.7
3NS mixture	Mean (mm/mm × 10^{-6})	4804.8	5285.7	5377.1	5642.4	5734.9
	Standard deviation (mm/mm × 10^{-6})	354.2	325.1	314.6	285.9	284.7
	Coefficient of variation (%)	7.4	6.2	5.9	5.1	5.0
4NS mixture	Mean (mm/mm × 10^{-6})	8206.2	8402.3	8438.4	8533.9	8581.7
	Standard deviation (mm/mm × 10^{-6})	835.5	850.1	853.2	859.8	869.9
	Coefficient of variation (%)	10.2	10.1	10.1	10.1	10.1
Autogenous shrinkage						
2NS mixture	Mean	555.9	1063.0	1210.6	1427.1	1724.2
	Standard deviation (SD)	145.2	146.8	143.9	140.9	143.5
	Coefficient of variation (CV)	26.1	13.8	11.9	9.9	8.3
3NS mixture	Mean	1115.7	1514.9	1605.9	1717.7	1890.6
	Standard deviation (SD)	216.5	275.9	278.2	311.9	353.2
	coefficient of variation (CV)	19.4	18.2	17.3	18.2	18.7
4NS mixture	Mean	2088.0	2426.4	2507.3	2609.7	2817.4
	Standard deviation (SD)	78.2	99.0	100.4	106.7	112.5
	Coefficient of variation (CV)	3.7	4.1	4.0	4.1	4.0

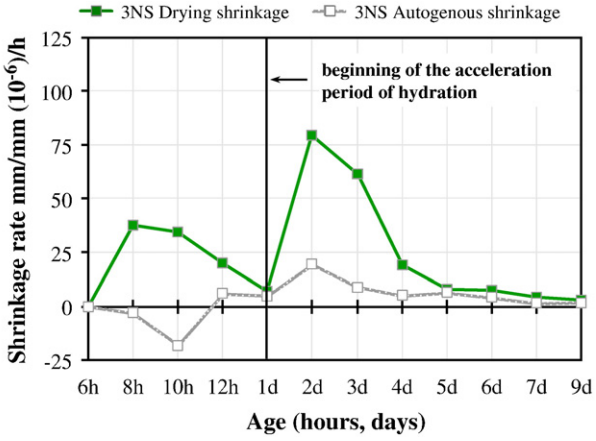

Fig. 11. Drying and autogenous shrinkage rates of 3NS mortars.

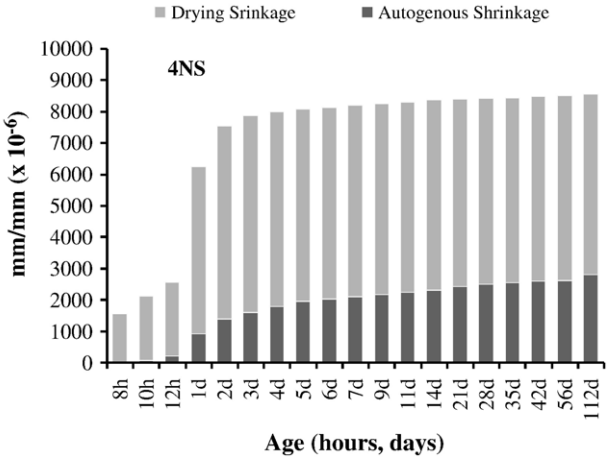

Fig. 13. Comparative graph of drying and autogenous shrinkage rate of 4NS mortar.

period begins, autogenous shrinkage rates vary with the amount of sodium silicate activator. Subsequently, mixtures 3NS and 2NS showed decreases in the autogenous shrinkage rate, even resulting in cumulative expansion. Due to fast hydration, the same behavior could not be detected for the 4NS mixtures.

The reabsorption of free water in the mixture is the most probable cause for the reported expansion observed in mixtures 3NS and 2NS; taking into account the expansion that happened immediately before the acceleration period of hydration. At this moment, the demand for water increases due to initial formation of C–S–H driving free water, bleeding water, to the sites where self-desiccation is more intense. This movement of water generates an increase in the relative humidity of the pores, diminishing the capillary tension that causes shrinkage.

The results of drying shrinkage rates for the three dosages of sodium silicate activator under consideration indicate the existence of an initial shrinkage peak followed by a second one, here designated “first shrinkage” and “second shrinkage”. The intensities of both peaks relate directly to the hydration kinetic and microstructure development of each mixture. The second drying shrinkage rate peak coincides accurately with the beginning of hydrated products formation for mixtures 2NS and 3NS as determined by calorimetry. The second drying shrinkage of mixture 4NS happens immediately after the beginning of the hydrated products formation. The expansion observed in autogenous shrinkage most likely contributes to the shrinkage rate reduction and the expansion observed in 2NS.

Evaporation of free water from macropores causes the first shrinkage rate peak, occurring immediately after demoulding. As hydration proceeds, the second drying shrinkage peak takes place and relates to the evaporation of water from mesopores and to the autogenous shrinkage that is intense at the beginning of the acceleration period of hydration. Autogenous shrinkage happens at the portion of the prism that does not lose water by evaporation. The beginning of the acceleration period of hydration and autogenous shrinkage practically coincide. This shows that during the induction period, both hydration and the formation of a more rigid microstructure are incipient [16], as well as chemical shrinkage and self-desiccation. Autogenous shrinkage increases rapidly as the hydration becomes more intense. As previously published [17], the increase of mesopores volume also coincides with the beginning of the

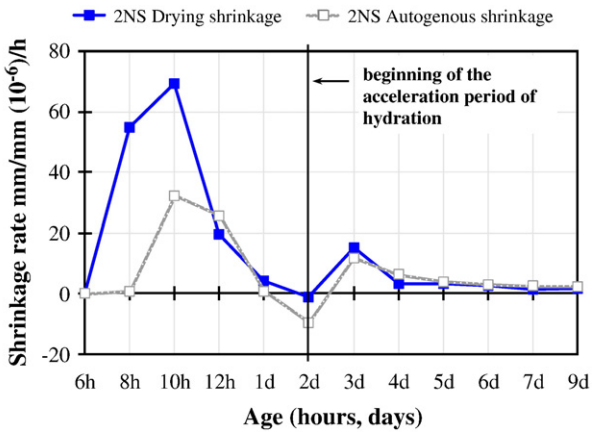

Fig. 12. Drying and autogenous shrinkage rates of 2NS mortars.

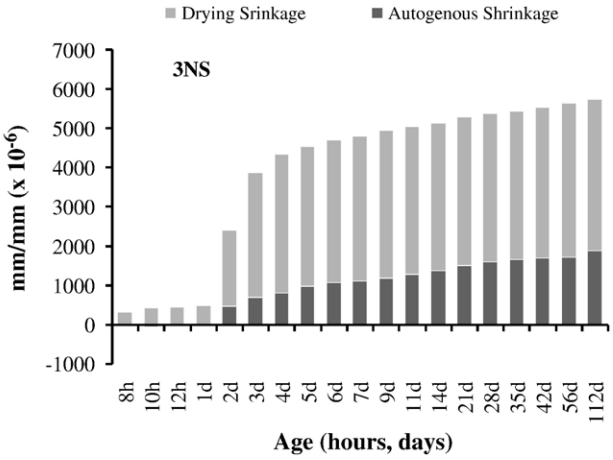

Fig. 14. Comparative graph of drying and autogenous shrinkage rate of 3NS mortar.

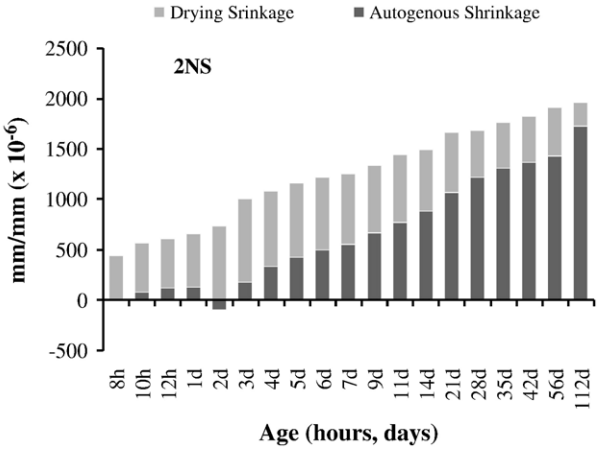

Fig. 15. Comparative graph of drying and autogenous shrinkage rate of 2NS mortar.

acceleration period of hydration. Nevertheless, a linear correlation between the evolution of autogenous shrinkage and the volume of mesopores appeared only for mixture 4NS (coefficient of correlation of 0.92).

The relation between autogenous shrinkage evolution and the volume of formed mesopores becomes less evident as the amount of silica diminishes in the activator [17]. The volume of mesopores does not fully correspond to the heat of hydration nor, the (TGA) weight loss associated with the degree of hydration for the pastes prepared with less silicate — mixtures 2NS and 3NS [17]. An increase in hydration heat is expected to produce a larger volume of formed mesopores and TGA weight loss correlating to the amount of C–S–H. All these parameters should relate to the extent of autogenous shrinkage. However, autogenous shrinkage increases even though the formation of mesopores diminishes. This apparent discrepancy most likely occurs because part of the hydrated products does not cause a refinement of the pores, but instead, the formation of inner particle hydrated products [19].

From a practical point of view, it is important to estimate the contribution of autogenous shrinkage to drying shrinkage, even though one could argue that the conditions, under which autogenous shrinkage occurs, in a wrapped sample and in the wet portion of drying shrinkage samples, are not the same. The autogenous shrinkage of mixture 4NS represents 30% of the drying shrinkage at 28 days (Fig. 13). For mixture 3NS, autogenous shrinkage starts at 2 days and represents 30% of the drying shrinkage at 28 days (Fig. 14). The contribution of autogenous shrinkage is more significant for mixture 2NS, representing 72% of the total drying shrinkage at 28 days, and 90% after 112 days (Fig. 15). Drying curve profiles are the same for all mixtures (Fig. 17), but the hydration of 2NS is slower (Fig. 11). Compared with mixtures 4NS and 3NS, mixture 2NS lost a greater amount of water due to evaporation during the drying condition, although, without having developed a significantly refined porous structure. This resulted in lower drying shrinkage. Mixture 2NS did not present any water loss due to environmental exposure during the autogenous condition, this favors an increase in autogenous shrinkage when compared with drying shrinkage.

3.5. Mass change characteristics and effect on drying shrinkage

Fig. 16 presents the mass changes during drying shrinkage testing and Fig. 17 the mass change rates. The profile of mass change rate curves is similar for all mixtures indicating that under exposure conditions of 24 °C and a relative humidity of 50%, water evaporation dynamics did not depend on the amount of sodium silicate in the activator. Nonetheless, the intensity and moment at which water evaporates is highly dependent on the activator content. A higher content of sodium silicate means less intense loss of water and a shorter period of water loss. Samples from mixture 4NS released less water through evaporation due to low porosity and more water consumed by hydration reactions. However, the amounts of water evaporated immediately after demoulding were the same for all mixtures.

Figs. 18, 19 and 20 present plots of drying shrinkage and mass change rates. The two curves are similar in mixture 4NS; the profile indicating that an initial release of water at demoulding causes the first shrinkage peak and autogenous shrinkage is most responsible for the second shrinkage peak.

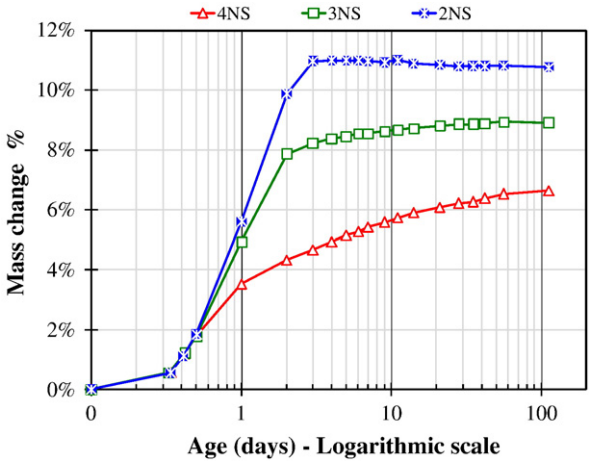

Fig. 16. Mass change of ASC mortars.

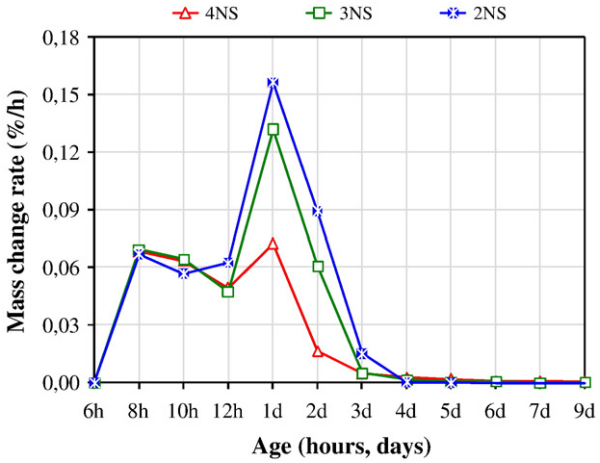

Fig. 17. Mass change rate of ASC mortars.

For mixtures 3NS and 2NS, only the profile of the first shrinkage rate peak coincides with the profile of the respective mass change rate curve. In mixture 2NS, the beginning of the acceleration period of hydration and a solid microstructure forms, only after 2 days. This produces a severe water loss immediately after demoulding (6 h) and drying shrinkage does not evolve accordingly. At the beginning of the second shrinkage rate peak, which corresponds with the beginning of the hydrated products formation, mixture 2NS has already lost most of the evaporable water and drying shrinkage proceeds less intensely. Autogenous shrinkage of the saturated portion of the drying shrinkage prisms is most likely responsible for the second shrinkage rate peak of mixture 2NS. In mixture 3NS, water evaporation occur during formation of the solid microstructure and refinement of porosity [17], producing an enhanced relation between the rates of drying shrinkage and water loss mass.

Collins and Sanjayan [22] advanced that the drying shrinkage of sodium silicate ASC is not entirely quantified by mass change. Adding to this conclusion, the results of this research indicate that the effect of mass change on shrinkage depends on the amount of sodium silicate in the activator. An increase in the amount of sodium silicate causes an increase in drying shrinkage, but a decrease in water mass loss due to evaporation (exposure at 6 h, at 24 °C and UR 50%). Early stage shrinkage is very intense in that the material is still soft. For the ASC, chemical shrinkage and hardening occur intensely, resulting in a high first shrinkage [17,20]. The results obtained in this work corroborate the increase in first drying shrinkage resulting from the larger amount of sodium silicate. This may be attributed to the effect of chemical shrinkage and the degree of hydration, which can be confirmed by the increase in the amount of C–S–H.

During the process of hardening deformations are reduced and consequently, external shrinkage also. However, there is a development of empty pores and menisci with an increase on capillary tension, resulting contraction forces and then shrinkage. ASC revealed a quick growth of voids and a wide range of mesopores, as previously observed [17,20,22]. This fact supports one of the explanations given for the high shrinkage of ASC since the pore size refinement [17,20,22] significantly contributes to the increase in capillary tension. According to the results obtained in this work, it can be concluded that increasing the amount of sodium silicate results in a large second shrinkage. Most probably, this is due to a decrease in total porosity and the extremely fast pore size refinement.

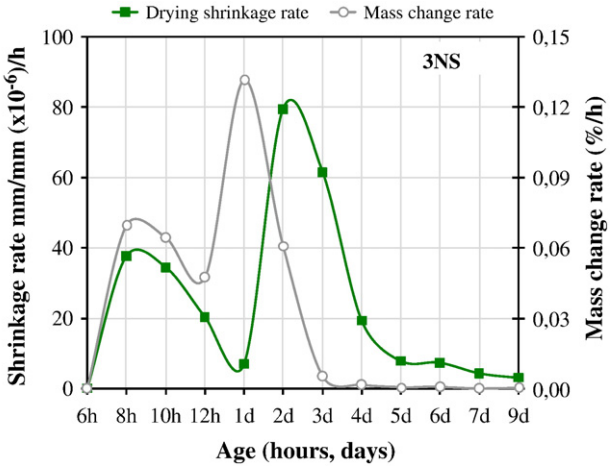

Fig. 19. Comparative graph of drying shrinkage and mass change rate of 3NS mortar.

4. Conclusions

The main conclusions of this study are:

- Activated slag cement (ASC) presents lower total porosity and higher volume of mesopores in direct relation to the content of activator. This characteristic is linked to a high degree of hydration and a predominant presence of C–S–H in the hydrated products.
- In drying shrinkage rate curves, two shrinkage rate peaks were visible, dubbed first and second shrinkages. The first peak results from a loss of water immediately after

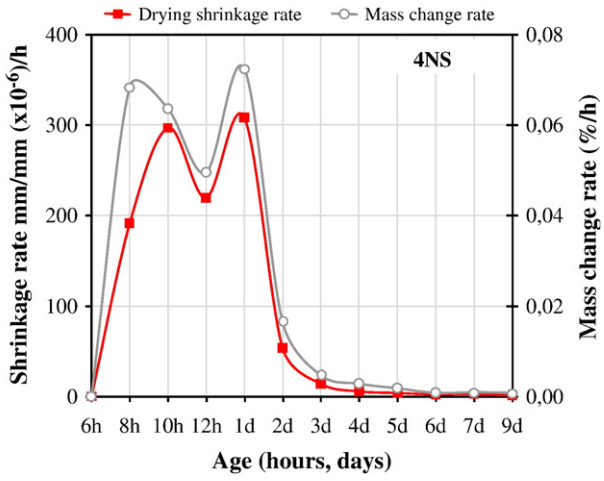

Fig. 18. Comparative graph of drying shrinkage and mass change rate of 4NS mortar.

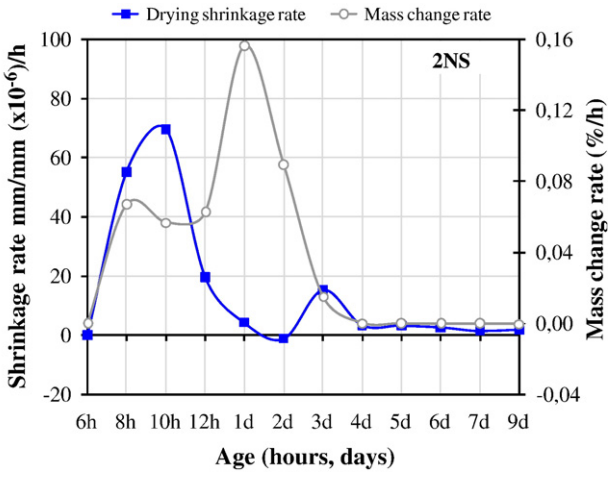

Fig. 20. Comparative graph of drying shrinkage and mass change rate for 2NS mortar.

demoulding. The second one occurs very near the initial formation of hydrated products and is responsible for the simultaneous effect of autogenous shrinkage and the deformation caused by evaporation.

- The amount of water released by evaporation is not the main reason for the high total shrinkage of ASC. As an example, mixture 4NS produced the highest drying shrinkage and lowest mass change. Second peak intensity decreases in the order, 2NS, 3NS, 4NS, illustrate the principal differences in mass change rate curves. Here, the intensity of water loss depends on the degree of hydration and porosity during the first three days.
- The amount of silicate contained in the activator plays an important role in autogenous and drying shrinkage. An increase in sodium silicate produces an increase in total shrinkage. Therefore, an increase in activator amount causes an increase in the degree of hydration, which results in an increase in C–S–H volume and accordingly, a decrease in porosity. These factors have a direct influence on the principal mechanisms of shrinkage.
- Results indicate that autogenous shrinkage is a significant part of the total dimensional changes observed for these cements. This can explain why the amount of water loss by evaporation does not account for the total measured shrinkage values.

Acknowledgments

The authors would like to thank the support from FAPESP (Fundação de Amparo à Pesquisa no Estado de São Paulo) and CNPq (Conselho Nacional de Desenvolvimento Científico e Tecnológico).

References

[1] D.M. Roy, Alkali-activated cements: opportunities and challenges, Cem. Concr. Res. 29 (2) (1999) 249–254.
[2] D.M. Roy, W. Jiang, M.R. Silsbee, Chloride diffusion in ordinary, blended, and alkali-activated cement pastes and its relation to other properties, Cem. Concr. Res. 30 (12) (2000) 1879–1884.
[3] A.A. Melo Neto Estudo da retração em argamassa de cimento de escória (Shrinkage of alkali-activated slag). São Paulo, 2002. 180p. (Master Science Thesis) — Escola Politécnica, Universidade de São Paulo. [in Portuguese].
[4] E. Douglas, A. Bilodeau, V.M. Malhotra, Properties and durability of alkali-activated slag concrete, ACI Mater. J. 89 (5) (1992) 509–516.
[5] V.M. John Cimentos de escória ativada com silicatos de sódio (Cements from slag activated with sodium silicate). São Paulo, 1995. 189p. (Doctor Thesis) — Escola Politécnica, Universidade de São Paulo. [in Portuguese].
[6] V.D. Glukhovsky, Ancient, modern and future concretes, 1st International Conference on Alkaline Cements and Concretes, Kiev, vol.1, 1994, pp. 1–9.
[7] C. Shi, J.A. Stegemann, Acid corrosion resistance of different cementing materials, Cem. Concr. Res. 30 (5) (2000) 803–808.
[8] F. Collins, J.G. Sanjayan, Microcracking and strength development of alkali activated slag concrete, Cem. Concr. Res. 23 (4–5) (2001) 345–352.
[9] S.D. Wang, X.C. Pu, K.L. Scrivener, P.L. Pratt, Alkali-activated slag cement and concrete: a review of properties and problems, Adv. Cem. Res. 7 (27) (1995) 93–102.
[10] H.F.W. Taylor, Cement Chemistry, 2th, ed, Thomas Telford House, 1997, p. 480.
[11] C. Shi, Strength, pore structure and permeability of alkali-activated slag mortars, Cem. Concr. Res. 26 (12) (1996) 1789–1799.
[12] C. Shi, R.L. Day, Some factors affecting early hydration of alkali-slag cements, Cem. Concr. Res. 26 (3) (1996) 439–447.
[13] T. Bakharev, J.G. Sanjayan, Y. Cheng, Alkali activation of Australian slag cements, Cem. Concr. Res. 29 (1) (1999) 113–120.
[14] R. Andersson, H.E. Gram, Properties of alkali-activated slag, Alkali Activated Slag (Part I), Swedish Cement and Concrete Research Institute, Stockholm, 1988, pp. 9–63, (CBI Research to 1–88).
[15] L. Yongde, S. Yao, Preliminary study on combined-alkali-slag paste materials, Cem. Concr. Res. 30 (6) (2000) 963–966.
[16] A.A. Melo Neto, W.L. Repette, M.A. Cincotto, Efeito do teor de ativador no desenvolvimento da resistência à compressão do cimento de escória ativada com silicato de sódio, Construção 2004: Repensar a Construção, 2004, Porto, Portugal, vol. 1, 2004, pp. 345–350.
[17] M.A. Cincotto, A.A. Melo Neto, W.L. Repette, Effect of different activators type and dosages and relation with autogenous shrinkage of activated blast furnace slag cement, International Congress on the Chemistry of Cement, 2003, pp. 1878–1888.
[18] A.F. Jiménez, F. Puertas, Alkali-activated slag cements: kinetic studies, Cem. Concr. Res. 27 (3) (1997) 359–368.
[19] A.R. Brough, A. Atkinson, Sodium silicate-based, alkali-activated slag mortars Part I. Strength, hydration and microstructure, Cem. Concr. Res. 32 (6) (2002) 865–879.
[20] W. Chen, H.J.H. Brouwers, The hydration of slag, part 1: reaction models for alkali-activated slag, J. Mater. Sci. 42 (2007) 428–443.
[21] T.C. Powers, T.L. Brownyard, Studies of the Physical Properties of Hardened Portland Cement Paste, Bulletin, vol. 22, Research Laboratories of the Portland Cement Association, Chicago, 1948.
[22] F.G. Collins, J.G. Sanjayan, Effect of pore size distribution on drying shrinkage of alkali-activated slag concrete, Cem. Concr. Res. 30 (9) (2000) 1401–1406.